Further Characterisation of Native Copper Inclusions in Cu-Bearing Tourmaline

Native copper inclusions have been reported in Cu-bearing gem tourmaline from Paraíba State in Brazil since its discovery in the late 1980s (Fritsch *et al.* 1990). Similar native copper inclusions have been found in other gem materials, such as Oregon sunstone (labradorite feldspar; e.g. Badur 2022). However, the native copper inclusions in Oregon sunstone generally have a more uniform size and distribution than those in copper-bearing tourmaline. Native copper inclusions in tourmaline have been mentioned in the literature only occasionally, probably since they are rather rare (Fritsch *et al.* 1990; Koivula *et al.* 1992; Brandstätter & Niedermayr 1994; Hartley 2018).

Brandstätter and Niedermayr (1994) observed thin, flat, gold-coloured dendritic inclusions of native copper extending parallel to the *c*-axis of Paraíba tourmaline, with the copper clusters scattered irregularly through the host crystal. Previously, Koivula *et al.* (1992) proposed a growth scenario for this type of inclusion as epigenetic exsolution from the host Cu-bearing tourmaline. That is, the inclusions formed along fractures in the host crystal after its crystallisation, with the copper being derived from the tourmaline rather than being added from external sources. Brandstätter and Niedermayr (1994) found that the CuO concentration in Paraíba tourmaline decreased towards the native copper inclusions. Thus, they also proposed epigenetic exsolution formation as being more plausible than syngenetic precipitation of native copper at the growing tourmaline's surface.

Recently, the authors investigated a crystal fragment of Cu-bearing elbaite from Paraíba State (Figure 12). This yellowish green to bluish green sample was reportedly untreated, and it contained up to 4,000 ppm Cu, as determined by laser ablation inductively coupled plasma time-of-flight mass spectrometry at SSEF. We observed numerous native copper inclusions in the sample (e.g. Figure 13a). The inclusions were clustered in a rather large planar area, and they showed mainly one orientation along the *c*-axis of the host tourmaline, with their planar surfaces being mostly parallel to one another. We also observed abundant transparent inclusions (Figure 13b) that showed a morphology and orientation similar to that of the native copper inclusions (e.g. Figure 14a). As far as we know, this type of transparent inclusion has not been reported previously in Cu-bearing tourmaline. We interpret these to be fluid inclusions because we occasionally observed round gas bubbles inside them.

To further characterise the native copper inclusions, we first used a focused ion beam scanning electron microscope (FIB-SEM) to expose the cross-section of one typical platelet inclusion. The backscattered electron

Figure 12: A crystal fragment of Cu-bearing elbaite, reportedly from Paraíba State in Brazil, was examined to study its copper-bearing inclusions. Photo by H. A. O. Wang.

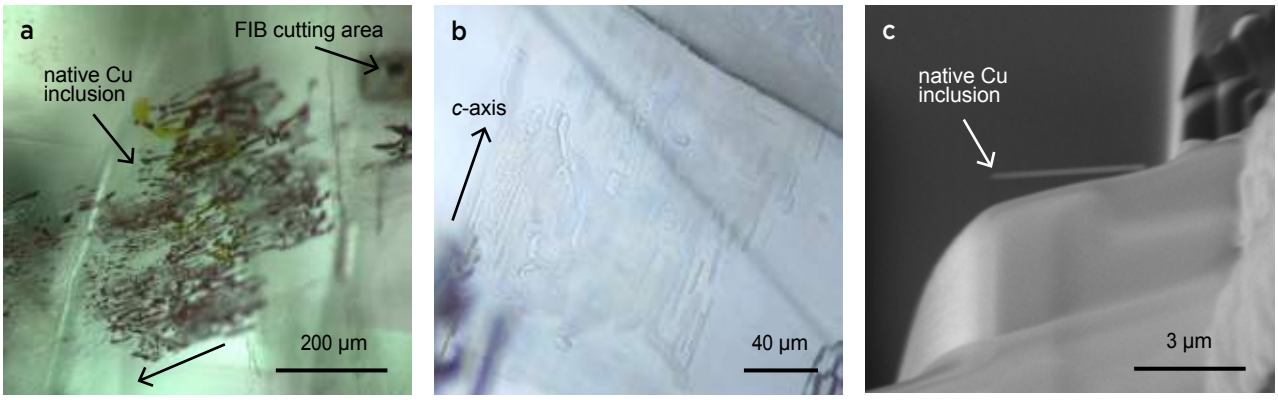

Figure 13: (**a**) A native copper inclusion in the tourmaline in Figure 12 is shown with an optical microscope using transmitted light. (**b**) Also present are occasional transparent inclusions with round gas bubbles and with a morphology similar to that of the native copper inclusions. (**c**) A backscattered electron (BSE) image of the cross-section of a native copper platelet shows a homogeneous thickness of about 150 nm. Photomicrographs by H. A. O. Wang and BSE image by D. Mathys.

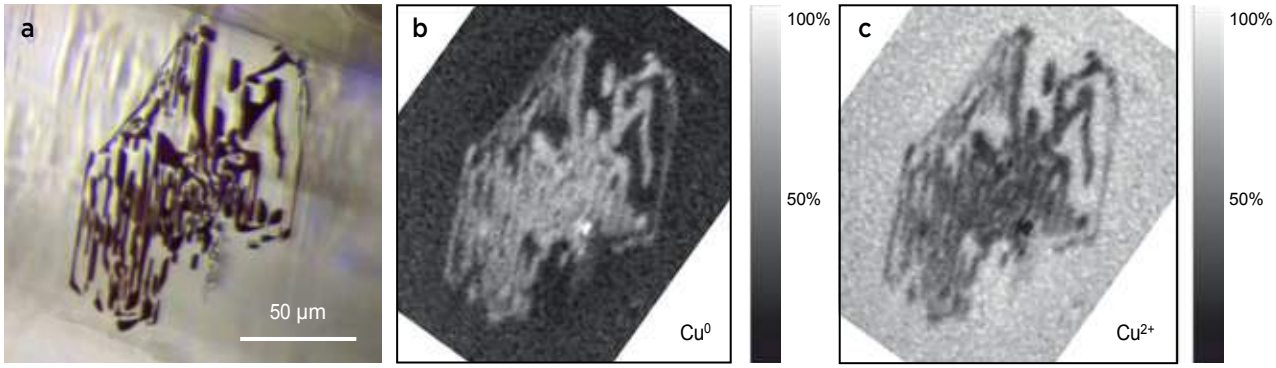

Figure 14: (**a**) Another native copper inclusion in the tourmaline in Figure 12 is seen here using an optical microscope with transmitted light. High-spatial-resolution redox maps of (**b**) metallic copper (Cu^0) and (**c**) oxidised copper (Cu^{2+}) are shown for the same view, and reveal that the inclusion consists of Cu^0 rather than Cu^{2+}. The scale on the right side of each map indicates the ratio of the corresponding Cu speciation to the total amount of copper. Photomicrograph by H. A. O. Wang and redox maps by D. Grolimund.

image of this inclusion is shown in Figure 13c; it had a thickness of about 150 nm and measured about 3–4 µm long. Interestingly, its length:thickness ratio was greater than that of native copper platelets in Oregon sunstone (as estimated from figures 11 and 14 in Badur 2022). To our knowledge, the gold-coloured platelet inclusions in Paraíba tourmaline were previously assumed to be composed of native copper, but without direct analytical evidence. Using spatially resolved synchrotron radiation X-ray absorption spectroscopy (specifically, micro-XANES), we revealed the characteristic local oxidation state of copper in a typical platelet inclusion and also in the host tourmaline. The chemical and electronic contrast revealed by this method can depict the electronic state of Cu (i.e. via copper 'redox maps'), including the distribution of metallic (Cu^0) and oxidised (Cu^{2+}) copper. Figure 14 shows these distributions for a typical inclusion located approximately 5 µm beneath the tourmaline's surface. The metallic Cu distribution in the redox maps (Figure 14b, c) correlates with the shape of the inclusion in the photomicrograph (Figure 14a), and shows that the copper is present as Cu^0. These results are the first direct proof that the gold-coloured platelet inclusions in Cu-bearing Paraíba tourmaline consist of native copper in its metallic state.

Additional observations, especially the presence of fluid inclusions with a morphology similar to that of the native copper inclusions, suggest that epigenetic exsolution might not easily explain the formation of this type of native copper inclusion. Instead, syngenetic (epitaxial) growth of native copper during the formation of the host tourmaline seems a more likely scenario. Nevertheless, we cannot fully exclude the formation of such inclusions as thin-film dendritic fracture-fillings after the formation of the host tourmaline, with the native copper being precipitated by fluid infiltration.

Further detailed research is ongoing to better understand these native copper inclusions in Brazilian Cu-bearing tourmaline. This study also demonstrates that cutting-edge micro-analytical methods new to gemmology (in this case, FIB-SEM and micro-XANES) have the potential to provide new insights to characterise gem materials and their formation.

Dr Hao A. O. Wang FGA *(gemlab@ssef.ch)*
Swiss Gemmological Institute SSEF
Basel, Switzerland

Dr Daniel Grolimund
microXAS Beamline, Swiss Light Source
Paul Scherrer Institute, Villigen, Switzerland

Prof. Dr Leander Franz
Department of Environmental Sciences
University of Basel, Switzerland

Daniel Mathys
Nano Imaging Lab, Swiss Nanoscience Institute
University of Basel, Switzerland

Prof. Dr Rainer Schultz-Güttler
Institute of Geosciences, University of São Paulo, Brazil

Dr Michael S. Krzemnicki FGA
Swiss Gemmological Institute SSEF and
Department of Environmental Sciences
University of Basel, Switzerland

References

Badur, C.B. 2022. *An investigation of native copper in plagioclase, Lake and Harney Counties, Oregon*. Master's thesis, Auburn University, Alabama, USA, 76 pp., https://etd.auburn.edu//handle/10415/8200.

Brandstätter, F. & Niedermayr, G. 1994. Copper and tenorite inclusions in cuprian-elbaite tourmaline from Paraíba, Brazil. *Gems & Gemology*, **30**(3), 178–183, https://doi.org/10.5741/gems.30.3.178.

Fritsch, E., Shigley, J.E., Rossman, G.R., Mercer, M.E., Muhlmeister, S.M. & Moon, M. 1990. Gem-quality cuprian-elbaite tourmalines from São José da Batalha, Paraíba, Brazil. *Gems & Gemology*, **26**(3), 189–205, https://doi.org/10.5741/gems.26.3.189.

Hartley, A. 2018. Gem Notes: Native copper inclusions in a Cu-bearing tourmaline. *Journal of Gemmology*, **36**(3), 203.

Koivula, J.I., Kammerling, R.C. & Fritsch, E. 1992. Gem News: Tourmaline with distinctive inclusions. *Gems & Gemology*, **28**(3), 204.

Photochromism and Phosphorescence of Tugtupite

Tugtupite belongs to the sodalite mineral group, with an ideal chemical formula of $Na_4BeAlSi_4O_{12}Cl$. It is named after its type locality at Tugtup Agtakôrfia in Greenland (Sørensen 1960). Tugtupite has been rarely used as a gem material since 1965 (Jensen & Petersen 1982). Almost all gem-quality tugtupite comes from the Taseq and Kvaneeld areas of the Ilímaussaq complex in Greenland. It is usually cut and polished into cabochons; faceted stones are seldom encountered due to the common presence of fractures and a distinct cleavage on {101}.

Tugtupite provides an example of a gem material that shows photochromism, meaning that it reversibly changes colour upon exposure to visible light or UV radiation (Blumentritt & Fritsch 2021). Specifically, it becomes dark red when exposed to UV radiation (or is irradiated by X-rays), and the colour fades to a paler red, pink or white when kept in the dark or exposed to bright light for a few minutes. This colour behaviour is probably due to an electron trapped in a Cl vacancy and associated sulphur polyanions (Blumentritt & Fritsch 2021).

Recently, the authors had an opportunity to examine a 1.76 ct faceted tugtupite. The stone had RIs of 1.497–1.500 (birefringence = 0.003), which is consistent with the literature (Jensen & Petersen 1982; Anthony *et al.* 1990). FTIR and Raman spectroscopy confirmed it was tugtupite. Microscopic observation revealed several colourless and irregular mineral crystals and fluid inclusions.

The stone was initially pink, and turned red immediately upon exposure to long-wave UV radiation (Figure 15). After the UV lamp was turned off, the stone returned to pink after several minutes. This chromatic change was repeatable. However, several small white parts of the sample showed no distinct change in colour (again, see Figure 15), and Raman analysis of those areas identified them as feldspar, which explains the absence of photochromism there.

Visible-near infrared (Vis-NIR) spectra were collected using a GEM 3000 spectrometer for both the pink and red colour states of the sample (Figure 16). In its pink state, the stone displayed two primary broad bands centred around 390 and 515 nm, with a weak band at approximately 700 nm. However, in its red state after exposure to UV radiation, the stone displayed only a single major band centred around 520 nm.

A SYNTHdetect diamond-screening instrument (McGuiness *et al.* 2020) was used to test the phosphorescence of the tugtupite sample, because this time-gated luminescence imaging system (with a UV source of < 220 nm) can detect very short-lived phosphorescence that usually cannot be seen with the unaided eye. We chose nine exposure delay times ranging from 11 to 40,000 µs (or 0.04 s) to demonstrate the sample's phosphorescence behaviour. The instrument recorded intense yellow phosphorescence that gradually faded to near-darkness during this time period (Figure 17, top row). A prominent red hue appeared at 4,700 µs, and the yellow was nearly gone at 17,000 µs. The overall phosphorescence faded distinctly at 30,000 µs and it could be barely seen at 40,000 µs.

Figure 15: This 1.76 ct faceted tugtupite turned from pink to red immediately when exposed to long-wave UV radiation of 365 nm. Stone courtesy of Xiaokang Xiong; composite photo by Huixin Zhao.